Hydrodynamics and Mass Transfer in a Turbulent Buoyant Bubbly Shear Layer

H. Ayed
Ecole Nationale des Ingénieurs de Tunis, Tunisia; and
Institut de Mécanique des Fluides de Toulouse, UMR5502, France

J. Chahed
Ecole Nationale des Ingénieurs de Tunis, Tunisia

V. Roig
Institut de Mécanique des Fluides de Toulouse, UMR5502, France

DOI 10.1002/aic.11290
Published online September 6, 2007 in Wiley InterScience (www.interscience.wiley.com).

Experimental analysis and numerical simulation of hydrodynamics and mass transfer in a turbulent oxygen–water bubbly shear layer is presented. The experimental data presents the structure of the averaged and fluctuating velocity fields as well as those of the gas volumetric fraction and the local dissolved oxygen concentration. Numerical simulations have been performed using Euler–Euler two-fluid model that provides some specific modeling adapted for gas–liquid bubbly flows and allows a reasonable representation of the two-phase flow structure (fields of average velocities and volumetric fractions of the two phases) as well as the important modulation of the turbulence in the two-phase flow. With the improvements of two-phase flow prediction, the averaged oxygen concentration field is also well predicted. The analysis of these results supports the pertinence of some improvements in two-phase flow modeling and allows some proposals for further progress in the development of more general multiphase models for complex gas–liquid systems. © 2007 American Institute of Chemical Engineers *AIChE J,* 53: 2742–2753, 2007

Keywords: bubbly flows, turbulence modeling, mass transfer, experiments, numerical simulation

Introduction

Gas–liquid bubbly systems are used in many industrial processes in order to perform mass and heat transfers. In these multiphase systems, the interfacial interactions and exchanges most often impose the technology of the process itself. Bubbly reactor processes include, for example, fermentation, bio-oxygenation, production of proteins, and wastewater treatment. In the classical bubbly reactors (bubble column, or gas-lift) the efficiency depends on the efficiency of the mixing and of the interfacial transfer rates. The mass and energy transfer depend on the diameters of the bubbles and on their velocities, as well as on the hydrodynamics of the liquid phase which ensures the dispersion of the bubbles. If chemical reactions occur in the liquid phase, the micromixing of the chemical species and their reaction are also strongly controlled by the hydrodynamics of the liquid phase. Moreover, industrial bubbly reactors may employ impellers, or complex geometrical configurations, which complicate the fluid dynamics. The optimization and the upgrade of these

Correspondence concerning this article should be addressed to V. Roig at veronique.roig@imft.fr.

industrial processes need a better knowledge of the physical mechanisms at the local scale (at the bubble scale typically). Local computational fluid dynamics (CFD) is thus a useful tool and the development of general models for gas–liquid systems represents a crucial interest.

A large theoretical, experimental, and numerical amount of research has been carried out on this subject during the two last decades. The research in the domain of bubbly flows has enhanced our understanding of the physical phenomena that control the interfacial interactions between the gas and the liquid phases and has contributed to the development of local two-fluid models applied to industrial gas–liquid systems.[1–3] In the models, the authors attempt to take into account the two-way coupling between the gas and liquid phases in order to represent the modification of the dynamics of the continuous liquid phase by the bubble presence. Despite the progress achieved in this field, some key-points of the two-fluid Euler–Euler models are still questionable. They are related, at first, to the accurate modeling of the turbulence in gas–liquid bubbly flows and especially to turbulent viscosity models.[4] The prediction of mass transfer and mixing of chemical species in bubbly flows is also still a challenge, mainly because the interfacial transfer rates in a bubble swarm do not follow the interfacial transfer laws valid for isolated bubbles in general. The mean relative velocity of bubbles in swarms and the mass transfer rate may be strongly modified by the interactions between the bubbles.[5,6]

On the other hand, experimental results on mass transfer and passive scalar mixing in bubbly flows are quite scarce because of the limitations of measurement methods in bubbly flows, especially when mass transfer is in concern. To produce local experimental data on gas–liquid mass transfer, new experiments in a turbulent buoyant bubbly shear layer were performed using the experimental set-up developed by Larue de Tournemine.[7] The bubbly flow is composed of oxygen as the gas phase and water as the continuous liquid one. We have characterized the local hydrodynamics of both phases as well as the local concentration of dissolved oxygen. The flow could be considered as representative of some industrial complexities that happen in industrial gas–liquid reactors. Indeed, because of the non-negligible void fraction, and to the nonhomogeneous injection of the bubbles, the dynamics of the flow involve a deep two-way coupling. Previous experimental investigation indicated that this flow configuration is deeply influenced by bubble-induced turbulence at small length scales.[8] The relative motion of the bubbles due to gravity is at the origin of this complex bubble-induced turbulence. On another side, due to the non homogeneous injection, the flow is also modified at the largest scales by buoyancy effects. In addition, the flow evolves gradually enough to allow detailed experimental investigation.

In the present contribution, numerical simulations have also been performed using Euler–Euler two-fluid modeling developed by Chahed et al.[9] and Bellakhal et al.[10–11] The turbulence modulation of the liquid phase due to the bubble presence is still an important issue in the closure of two-fluid model equations. Sato et al.[12] and Lopez de Bertodano et al.[13] have proposed specific models that modify the eddy viscosity of the liquid phase because of the relative movements of the bubbles. But these models are limited and can only predict increases of the eddy viscosity because of the influence of the bubbles, whereas some experimental results show that a decrease of the eddy viscosity can also be observed due to the presence of the bubbles.[14] In the present model, the turbulence closure is based on a separation of the shear-induced turbulence and bubble-induced turbulence for which specific transport equations are modeled. In this model, two time scales are involved in the turbulent transport. As in single-phase flow, a time scale related to the eddy stretching and, specific to two-phase flow, a time scale related to the bubble relative movements. This turbulence closure leads to the development of second order and first order turbulence models that succeeded in reproducing the experimental data in many basic turbulent bubbly flows with low and moderate void fractions (homogeneous turbulence, shear layers,[9] and wall-bounded bubbly flows[15]).

Another crucial point in bubbly flow modeling concerns the formulation of the interfacial momentum exchange. The distribution of the void fraction in nonhomogeneous bubbly flows is controlled by the force exerted by the continuous phase on the bubbles as they move throughout the liquid. The averaged force depends on the averaged and fluctuating flow fields of the liquid and of the gas. The turbulent contribution to the interfacial momentum transfer is not often modeled, while it can be essential in the prediction of the bubbles distribution.[16–19] In the present two-fluid model, the turbulent contribution of the added mass force to the interfacial momentum transfer term is taken into account following Chahed et al.[15]

Finally, when mass transfer is in concern, the transport equation of a passive scalar (here the dissolved oxygen concentration in the liquid) requires closures for the turbulent transport in the bulk of the continuous phase and for mass transfer through the gas–liquid interface. In this article we test a specific model for the turbulent diffusivity of the concentration. The mass transfer rate is proportional to the local volumetric interfacial area which is the surface of the interface per unit volume. So, for fixed size and shape of the bubbles, the accurate prediction of the phase distribution is essential for its estimation. We have thus tested the effect of various closure laws for the interfacial momentum transfer on the global prediction of the flow. The global transfer rate coefficient also involves a local time scale related to interface renewal. This time scale could depend on the turbulence structure at the scale of the bubble, but the present knowledge about the turbulence effects on the mass transfer around an isolated bubble, as well as the knowledge about the turbulence structure inside a swarm of bubbles, is far too limited to build a mass transfer model for a bubble in a swarm. In this contribution, we have thus considered that the mass transfer coefficient is given by an empirical correlation or by Higbie's relation.

Eulerian–Eulerian Two-Fluid Model for Turbulent Gas–Liquid Bubbly Flows

The Eulerian–Eulerian two-fluid model proposed in Chahed et al.[9,15,20] (with different levels of the turbulence closures) provides some specific modeling adapted for gas–liquid bubbly flows. The turbulence modeling has been improved to take into account the bubble-induced turbulence, and the interfacial momentum transfer is better described, including a turbulent contribution of the added mass forces. This two-fluid model allows an accurate representation of the

velocity fields and of the void fraction in basic bubbly flows with moderate void fractions. It has been tested successfully up to 10% of void fraction. In this article, we use this model for the prediction of mass transfer in gas–liquid systems. We first present the two-fluid model equations and we then describe the closure laws that we have used for the transport equations (momentum, turbulence, and passive scalar).

Basic equations of the two-fluid model

We note $\alpha = <\chi_G>$ the void fraction which represents the volumetric fraction of gas obtained by applying ensemble averaging to the characteristic function $\chi_G(x_i,t)$ of the gas phase ($\chi_G(x_i,t)=1$ in the gas phase and $\chi_G(x_i,t)=0$ elsewhere). Neglecting the interface thickness, we may express the characteristic function of the liquid as $\chi_L(x_i,t) = 1-\chi_G(x_i,t)$. Thus, $(1-\alpha) = <\chi_L(x_i,t)>$ is the volume fraction of the liquid phase. We note u_{Li}, p_L, ρ_L, respectively, the i component of the liquid velocity, the pressure, and the density of the liquid phase. With the subscript G these variables are related to the gas phase. We define for each eulerian variable $\varphi_k(x_i,t)$ in the phase k (k = L or G), the average value $\overline{\overline{\varphi_k}}$ in the phase k as: $\alpha_k\overline{\overline{\varphi_k}} = <\chi_k\varphi_k>$ and its fluctuation $\varphi'_k = \varphi_k - \overline{\overline{\varphi_k}}$ where $<.>$ means ensemble averaging.

We consider turbulent gas–liquid bubbly flow with low solubility of the gas in the liquid. So that we may consider that mass transfer has no effect on the mass and momentum balances. We assume that no coalescence or break-up occur, in these conditions we consider that the bubble diameter is still roughly constant.

The mass and momentum balances averaged in the liquid and the gas phase are thus given by the following relations.

In the liquid:

$$\frac{\partial}{\partial t}((1-\alpha)\rho_L) + \frac{\partial}{\partial x_i}((1-\alpha)\rho_L\overline{\overline{u_{Li}}}) = 0 \tag{1}$$

$$\rho_L(1-\alpha)\frac{D\overline{\overline{u_{Li}}}}{Dt} = (1-\alpha)\frac{\partial}{\partial x_j}\overline{\overline{\sigma_{Lij}}} - \rho_L\frac{\partial}{\partial x_j}\left[\left(1-\alpha\right)\overline{\overline{u'_{Li}u'_{Lj}}}\right] + \rho_L(1-\alpha)g_i - M_{Gi} \tag{2}$$

In the gas:

$$\frac{\partial}{\partial t}(\alpha\rho_G) + \frac{\partial}{\partial x_i}(\alpha\rho_G\overline{\overline{u_{Gi}}}) = 0 \tag{3}$$

$$\rho_G\alpha\frac{d\overline{\overline{u_{Gi}}}}{dt} = \alpha\frac{\partial}{\partial x_j}\overline{\overline{\sigma_{Gij}}} - \rho_G\frac{\partial}{\partial x_j}\left[\alpha\overline{\overline{u'_{Gi}u'_{Gj}}}\right] + \rho_G\alpha g_i + M_{Gi} \tag{4}$$

where $\frac{D}{Dt} = \frac{\partial}{\partial t} + \overline{\overline{u_{Li}}}\frac{\partial}{\partial x_i}$ and $\frac{d}{dt} = \frac{\partial}{\partial t} + \overline{\overline{u_{Gi}}}\frac{\partial}{\partial x_i}$ are respectively the material derivatives according to the liquid and to the gas mean velocities. σ_{Lij} and σ_{Gij} are respectively the stress tensor of the liquid and of the gas. For Newtonian fluids they write $\overline{\overline{\sigma_{kij}}} = -\overline{\overline{p_k}}\delta_{ij} + 2\mu_k\left[\frac{\partial\overline{\overline{u_{ki}}}}{\partial x_j} + \frac{\partial\overline{\overline{u_{kj}}}}{\partial x_i}\right]$ where μ_k is the dynamic molecular viscosity; $\overline{\overline{u'_{Li}u'_{Lj}}}$ and $\overline{\overline{u'_{Gi}u'_{Gj}}}$ are the Reynolds stress tensors of the liquid and of the gas and M_{Gi} is the ith component of the interfacial momentum transfer rate from the gas to the liquid.

If we neglect the density of the gas in comparison with the density of the liquid, Eq. 4 indicate that the total local density of the force exerted on the bubbles is zero. This equation is written in the form:

$$0 = \alpha\frac{\partial}{\partial x_j}\overline{\overline{\sigma^{(0)}_{Lij}}} + M_{Gi} \tag{5}$$

where $\sigma^{(0)}_{Lij}$ is the liquid stress field of the "nonperturbed" flow and the interfacial momentum exchange M_{Gi} represents the contribution of the "disturbed" flow.[21,22] The "nonperturbed" contribution would be present even in the absence of any material interface, it is identified here to the action of the local shear stress of the continuous phase $\left(\overline{\overline{\sigma^{(0)}_{Lij}}} \equiv \overline{\overline{\sigma_{Lij}}}\right)$.

Equations 1–4 represent the basic equations of the two-fluid model. This model requires closures for the Reynolds stress tensors of the liquid and gas phases, $\overline{\overline{u'_{Li}u'_{Lj}}}$ and $\overline{\overline{u'_{Gi}u'_{Gj}}}$, and for the momentum transfer term M_{Gi}.

Closure of the two-fluid model

Interfacial Momentum Transfer Modeling. As mentioned earlier, the interfacial momentum exchange M_{Gi} corresponds to the contribution of the "disturbed" flow around the bubbles to the density of the total force exerted by the liquid on the bubble. The interfacial momentum transfer term is written by averaging the force exerted by the fluid on the bubbles. In the common formulation of the momentum interfacial exchange, only the contributions due to the averaged velocity fields of the liquid and of the gas phases are considered while the turbulent contributions of the interfacial force are ignored, or eventually expressed via a supplementary dispersion term proportional to the void fraction gradient.[18] A previous experimental analysis of bubbly pipe flow in microgravity conditions showed that these models are incomplete, and that a nonlinear added mass term improves greatly the closure law of the momentum transfer.[15] This term comprises a diffusion effect proportional to the void fraction gradient which may be interpreted as a drift velocity.[19] The formulation for the average density (per unit volume) of the force exerted by the fluid on the bubbles is then modeled as follows:

$$M_{Gi} = -\frac{3}{4}\alpha\rho_L\frac{C_D}{d}\|\overline{\overline{u_R}}\|\overline{\overline{u_{Ri}}} - 2\alpha\rho_L C_{LF}\overline{\overline{\omega_{Lij}}}\times\overline{\overline{u_{Rj}}} - \alpha\rho_L C_A\left(\frac{d}{dt}\overline{\overline{u_{Gi}}} - \frac{D}{Dt}\overline{\overline{u_{Li}}}\right) - \rho_L C_A\frac{\partial}{\partial x_j}\left[\alpha(\overline{\overline{u'_{Gi}u'_{Gj}}} - \overline{\overline{u'_{Li}u'_{Lj}}})\right] \tag{6}$$

This interfacial momentum transfer model contains respectively the well known drag (coefficient C_D), added mass (coefficient C_A), and lift (coefficient C_{LF}) averaged forces and a specific turbulent term which comes from the averaging of the added mass term (last term).

Turbulence Modeling. The turbulence closure is based on a "three-equations" turbulence model developed for turbulent bubbly flows and described in details in Bellakhal et al.[10] It consists in a reduction of a second order turbulence model discussed in Chahed et al.[9] In this model, the Reynolds stress tensor of the continuous phase is split into two parts which are assumed statistically independent: a turbulent part produced by the gradient of the mean velocity and by the

bubbles' wakes denoted $\overline{\overline{u'_{Li}u'_{Lj}(0)}}$, and a pseudo-turbulent part induced by the bubbles displacements and controlled by the added-mass effects denoted $\overline{\overline{u'_{Li}u'_{Lj}(S)}}$. We thus write:

$$\overline{\overline{u'_{Li}u'_{Lj}}} = \overline{\overline{u'_{Li}u'_{Lj}(0)}} + \overline{\overline{u'_{Li}u'_{Lj}(S)}}$$

Both components of the Reynolds stress tensor are modeled using specific transport equations. In this second order turbulence model, two time scales are involved in the turbulent transport. A time scale related to the eddy stretching $\tau_t = \frac{k_0}{\varepsilon_0}$ and a time scale related to the bubble relative movements $\tau_b = C_R \frac{d}{U_R}$. C_R is a constant which has been adjusted from the experimental data in homogeneous turbulence with uniform shear.[9]

According to the second order turbulence closure, the simplified balance between production and redistribution in the shear stress transport equation allows the formulation of an original expression of the turbulent viscosity in bubbly flow in the form:

$$\nu_t = C_{\mu 0}\frac{k_0^2}{\varepsilon_0}\frac{(1+\frac{C_{\mu b}}{C_{\mu 0}}\frac{k_s}{k_0})}{(1+\alpha\frac{\tau_t}{\tau_b})} = \nu_{t0}\frac{(1+\frac{C_{\mu b}}{C_{\mu 0}}\frac{k_s}{k_0})}{(1+\alpha\frac{\tau_t}{\tau_b})} \tag{7}$$

where $C_{\mu 0}$ and $C_{\mu b}$ are coefficients depending on the turbulence and pseudo-turbulence anisotropy. The ratio of these coefficients is of order of unity. We note $\nu_{to} = C_{\mu 0}\frac{k_0^2}{\varepsilon_0}$ and take $C_{\mu 0}$ equal to 0.09 as in single-phase flow turbulence modeling. It should be observed that for dispersed phase with small relative velocity or very low void fraction, the pseudo-turbulence is weak and Eq. 7 gives the turbulent viscosity of the equivalent single-phase flow ν_{to}.

The turbulent viscosity formulation (Eq. 7) expresses two effects of the bubbles agitation on the turbulent viscosity: the bubbles agitation induces on one hand an enhancement of the turbulent viscosity and on the other hand a modification of the eddies stretching characteristic scale that causes more isotropy of the turbulence with an attenuation of the shear stress (denominator of Eq. 7). As a result, depending on which of these two effects dominates, the turbulent shear stress in bubbly flow can be more or less important than the corresponding one in the equivalent single-phase flow. In the case where the turbulent shear stress is reduced, the turbulence production by the mean velocity gradient is lower and we can expect, under certain conditions, an attenuation of the turbulence as observed in some wall bounded bubbly flows.[14,23]

On the basis of this turbulent viscosity formulation, a first order closure is developed.[11] The turbulent part of the Reynolds stress tensor is thus expressed using the turbulent viscosity concept according to Boussinesq hypothesis:

$$\overline{\overline{u'_{Li}u'_{Lj}(0)}} = -\nu_t\left[\frac{\partial\overline{\overline{u_{Li}}}}{\partial x_j} + \frac{\partial\overline{\overline{u_{Lj}}}}{\partial x_i}\right] + \frac{2}{3}k_0\delta_{ij}$$

The transport equation of the turbulent kinetic energy $k_0 = \frac{1}{2}\overline{\overline{u'_{Li}u'_{Li}(0)}}$ is deduced from second order closure developed in a formal way quite similar to single-phase flow closure procedures, except that specific interfacial effects are taken into account.

The pseudo-turbulent contribution is based on a theoretical solution in potential homogenous bubbly flow given by Biesheuvel and van Wijngaarden,[24] and the fluctuations are attributed to the added mass effects. According to their analysis we take:

$$\overline{\overline{u'_{Li}u'_{Lj}(S)}} = \tfrac{1}{5}\begin{bmatrix}4&0&0\\0&3&0\\0&0&3\end{bmatrix}k_s$$

in (x, y, z) coordinates, where $k_s = \frac{1}{2}\overline{\overline{u'_{Li}u'_{Li}(s)}}$ is the kinetic energy of the pseudo-turbulence and z is the vertical direction aligned with the mean relative velocity. The model for the transport equation of k_s is discussed in the following.

The modeled transport equations of the turbulent energy k_0, of the viscous dissipation rate ε_0, and of the pseudo-turbulent energy k_s are written as in Bellakhal et al.[11]:

$$\frac{D}{Dt}k_0 = \frac{C_{sk}}{(1-\alpha)}\frac{\partial}{\partial x_j}\left[(1-\alpha)(\tau_t k_0 + \tau_b k_s)\frac{\partial k_0}{\partial x_j}\right] + \nu_t\frac{\partial\overline{\overline{u_i}}}{\partial x_j}\left(\frac{\partial\overline{\overline{u_i}}}{\partial x_j} + \frac{\partial\overline{\overline{u_j}}}{\partial x_i}\right) - \varepsilon_0 \tag{8}$$

$$\frac{D}{Dt}\varepsilon_0 = \frac{C_{s\varepsilon}}{(1-\alpha)}\frac{\partial}{\partial x_j}\left[(1-\alpha)(\tau_t k_0 + \tau_b k_s)\frac{\partial \varepsilon_0}{\partial x_j}\right] + \frac{\varepsilon_0}{k_0}\left(C_{1\varepsilon}\nu_t\frac{\partial\overline{\overline{u_i}}}{\partial x_j}\left(\frac{\partial\overline{\overline{u_i}}}{\partial x_j} + \frac{\partial u_j}{\partial x_i}\right) - C_{2\varepsilon}\varepsilon_0\right) \tag{9}$$

$$\frac{D}{Dt}k_s = \frac{C_{sk}}{(1-\alpha)}\frac{\partial}{\partial x_j}\left[(1-\alpha)(\tau_t k_0 + \tau_b k_s)\frac{\partial k_s}{\partial x_j}\right] + \frac{C_A}{2}\frac{D}{Dt}\left(\alpha|\overrightarrow{u_R}|^2\right) \tag{10}$$

In the transport equations, the diffusion terms are modeled using a gradient law with a diffusion coefficient which includes the equivalent single-phase turbulent effect $C_{s\phi}\tau_t k_0 = \frac{\nu_{t0}}{\sigma_\phi}$, and a supplementary diffusivity due to the bubbles displacements, $\frac{\nu_b}{\sigma_\phi} = C_{s\phi}\tau_b k_s \approx \frac{C_b}{\sigma_\phi}\alpha d U_R$, that agrees with the expression proposed by Sato et al.[12] This model for diffusion also comes from a reduction of the second order general closure of the diffusion term in which the two time scales (τ_t and τ_b) were introduced. We may notice once more that for a dispersed phase with small relative velocity or very low void fraction, the diffusion term reduces to the single-phase model.

The transport equations of the turbulent part (Eq. 8) for the kinetic energy and (Eq. 9) of the viscous dissipation rate are formally quite similar to single-phase flow turbulence model but the diffusion and production terms take into account the interfacial effects. Moreover, the interfacial transfer of energy due to the power developed by the mean drag force in the relative movement does not appear explicitly in these relations because we have adopted as an assumption the suggestion of Lance and Bataille[25] of equilibrium between the production in the wakes with the extra-dissipation in the wakes. ε_0 is thus the dissipation at the small scales resulting from the energetic cascade.

Table 1. Coefficients for the Turbulence Model

C_R	0.67
$C_{\mu 0}$	0.09
$C_{\mu b}$	0.09
σ_k	1.0
σ_ε	1.3
$C_{1\varepsilon}$	1.44
$C_{2\varepsilon}$	1.92
σ_c	0.75

The last term in the right hand side of Eq. 10 for the pseudo-turbulent kinetic energy thus represents the interfacial production due to added mass forces in the relative movements. Equation 10 allows the advection and the diffusion, without dissipation of this bubble-induced kinetic energy produced by the relative movements.

The constants of the turbulence model have the values currently adopted for single-phase turbulence closure. The various coefficients introduced in the turbulent closure laws are reported in Table 1.

Transport Equation of Oxygen Concentration. The transport equation of a passive scalar requires closures for the turbulent transport and for mass transfer through the gas–liquid interface. Using the turbulent diffusion model presented earlier, the transport equation of the oxygen concentration in the liquid $\overline{C}_L$ is modeled as follows:

$$\frac{D}{Dt}\overline{C}_L = \frac{C_{sc}}{(1-\alpha)}\frac{\partial}{\partial x_j}\left[(1-\alpha)(\tau_t k_0 + \tau_b k_s)\frac{\partial \overline{C}_L}{\partial x_j}\right] + S_c \quad (11)$$

The left hand side term represents the mean flow convection; on the right-hand side we have respectively the diffusion term and the interfacial mass transfer term. There are numerous formulations of mass transfer in gas–liquid flow. All of them come down to a general formulation of the general mass flux:

$$S_c = k_L a(C_L^* - \overline{C}_L) \quad (12)$$

where k_L is the transfer coefficient, C_L^* is the concentration of oxygen in the liquid at saturation, a is the interfacial area, which is the surface of the interfaces per unit volume, and $\overline{C}_L$ the concentration far away from the interfaces. In monodisperse bubbly flows with spherical bubbles, the volumetric interfacial area is proportional to the void fraction and inversely proportional to the bubble diameter ($a = \frac{6\alpha}{d}$) which indicates the important role of the bubble diameter and of its distribution in the computation of the local mass transfer. Neglecting the curvature effects, we equate the pressures in both phases and Henry's law for pure oxygen bubbles gives: $C_L^* = \frac{P_L}{H}$ with $H = 74.68$ MPa l/mol.

As a model of the transfer coefficient k_L we have used the relation given by Brauer[26] (in Mewes and Wiemann[27]). It relates the Sherwood number $\mathrm{Sh} = \frac{k_L d}{D}$ to the Reynolds number of the relative movement $\mathrm{Re} = \frac{U_R d}{\nu}$ and to the Schmidt number $\mathrm{Sc} = \frac{\nu}{D}$. The diameter of the bubbles is denoted d, U_R their relative velocity, ν the molecular viscosity, and D is the gas–liquid diffusivity ($D = 2.2 \times 10^{-9}$ m^2 s^{-2} for oxygen in water). We thus take:

$$\mathrm{Sh} = \mathrm{Sh}_\infty\left[\left(1 + 0.433\,\mathrm{Re}^2\right)^{-1} + 4.23\right]^{-0.055}$$
$$\text{with } \mathrm{Sh}_\infty = 2 + \frac{0.651(\mathrm{Re\,Sc})^{1.72}}{1 + (\mathrm{Re\,Sc})^{1.22}} \quad (13)$$

Experimental Study

Experimental set up

The experiment set-up that we used is a quite general set-up developed to study bubbly flows from homogeneous ones to shear layers configurations.[7] It is described in details in Roig and Larue de Tournemine.[28] It consists of a vertical square section channel (0.3×0.15 m^2) of 3 m length, where the upward gas-water flows develop. It is operated at ambient pressure and temperature conditions. At the entrance of this channel, the inlet section is divided into two independent feeding systems on both sides of a splitter plate (2.5 mm of thickness). They consist of 0.15×0.15 m^2 sections, where 576 capillary tubes (0.33 mm internal diameter) generate the bubbles. The injectors are uniformly spaced with a distance between two injectors of 6 mm. In the present experiments the gas was pure oxygen. In each feeding system, the gas and liquid flow rates can be adjusted independently. We can perform bubbly flows with void fraction up to 20% and liquid velocities up to 1 m/s. Water circulates in a closed loop. It is pumped from an underground reserve of capacity 400 m^3, sufficiently large to ensure the stabilization of the temperature and of the concentration of dissolved oxygen during the experimentation.

The experimental conditions reported in this article are described in Table 2. The flow is a mixing layer with a liquid flow (water) in the high velocity side, and a gas–liquid (oxygen–water) bubbly flow in the low velocity side (see Figure 1 for a schematic diagram of the experimental conditions). The coordinate system is described in Figure 1. The inlet section is located at $x = 0$. Visual observation confirms that the flow is 2D in the vertical (x,y) plane (Figure 2).

Measurements have been performed at various longitudinal and transversal positions in order to investigate the spatial development of the flow. We report on Figure 3 the measured mean diameters and rms values of the diameters of the bubbles. These diameters evolve in a small range. The associated relative motions are at Reynolds numbers of about 500 based on the terminal velocity and bubble diameter. A transport model for the interfacial area would be interesting to test whether the mass transfer is sensitive to these variations. In the present contribution we consider that the sizes of the bubbles are constant.

Measurement methods

Measurement methods for hydrodynamic characterization have been developed in our laboratory for several years. We use classically a hot film for the measurements of the vertical velocity of the liquid $u_{Lx}(t)$, and a double optical fibber probe

Table 2. Experimental Inlet Conditions

Liquid velocity at the inlet, side 1	0.57 m/s
Liquid velocity at the inlet, side 2	0.29 m/s
Mean void fraction, side 1	0
Mean void fraction, side 2	2%

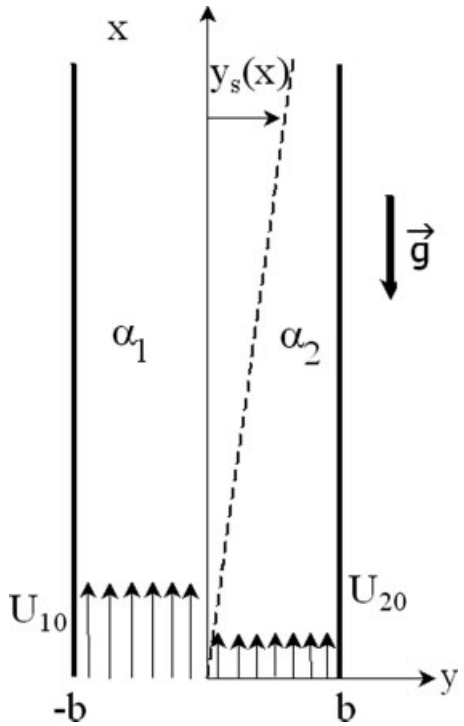

Figure 1. Schematic diagram of the experimental conditions (y_s is the visual frontier of the bubbly flow).

for the measurement of the vertical velocity of the bubbles, of their sizes and of the void fraction.[28,29] The bubbles diameters are estimated from the chords intercepted by the optical probe, assuming a spherical shape.[30]

Figure 2. View of a bubbly shear layer flow similar to the present case.

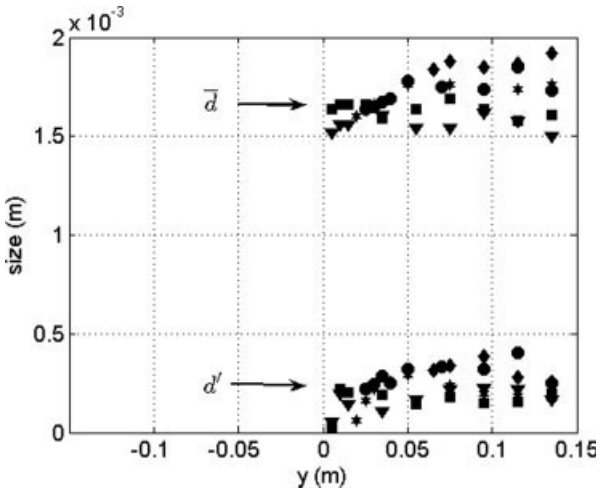

Figure 3. Average and rms bubble diameter measured in the bubbly mixing layer.

x = 5 cm ▼, 20 cm ■, 50 cm ★, 80 cm ●, 120 cm ◆.

In this present work, original local experimental measurements of the dissolved oxygen concentration in the liquid were performed. The measurements were made using an Unisense local probe. The Unisense oxygen probe is a Clark-type oxygen microsensor with a miniature sensitive tip (diameter of 20–30 μm) which makes it possible to make high spatial resolution measurements. In return, the temporal resolution of this probe is limited, so that we have just access to the averaged values of the dissolved oxygen concentration.

Results and Discussion

The numerical simulations have been performed after implementation of our closure model in the two-dimensional eulerian code Melodif developed by EdF.[17,31–33] It is based on finite difference discretization. The vertical length of the computational domain is 3 m long and the transverse length is 0.3 m. The discrete grid has 101 longitudinal nodes and 91 transverse nodes. We made preliminary tests to ensure that the solution was independent of the grid. Wall conditions are applied on the lateral boundaries, the upper boundary is an outlet boundary. The inlet section for the calculus corresponds to a real section located 0.05 m downstream of the splitter plate. The mean velocities of the liquid ($\overline{\overline{u_{Lx}}}_{\text{exp}}$) and of the bubbles, the void fraction and the concentration of dissolved oxygen are given from experiments at this inlet section. Turbulent inlet conditions are defined as explained in the following. Measurements give access only to the variance of the longitudinal velocity $(\overline{\overline{u'^2_{Lx}}})_{\text{exp}}$, while we have to give k_0, k_s, and ε_0. To prescribe the turbulent part k_0, we use a turbulent intensity profile $It_{\text{sp}}(y) = \sqrt{k}/\overline{\overline{u}}$ obtained from a single-phase flow simulation. We assume that the turbulent intensity is similar in both flows at the entrance, and we take for the bubbly case $k_0 = It^2_{\text{sp}}\overline{\overline{u_{Lx}}}^2_{\text{exp}}$. Then the dissipation rate ε_0 is prescribed by $\nu_{t0} = 150\nu$ which proved to lead to a good prediction of the single-phase flow development as compared to experiments (not shown here). We take $k = k_0 + k_s = \frac{3}{2}(\overline{\overline{u'^2_{Lx}}})_{\text{exp}}$, which gives us the inlet conditions for the pseudo-turbulent part k_S.

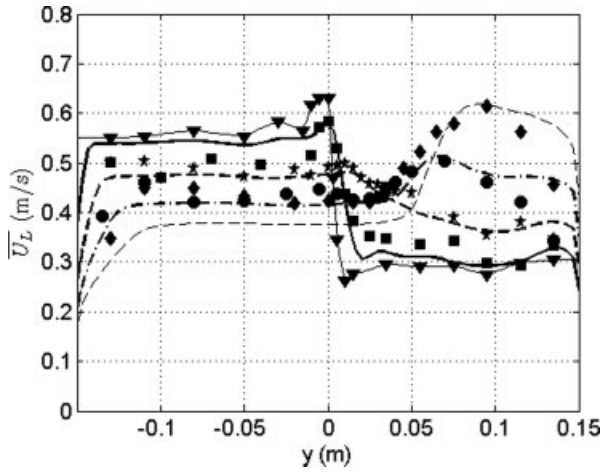

Figure 4. Liquid mean velocity profiles in the bubbly mixing layer.

Symbols, experimental results; lines, numerical prediction. x = 5 cm ▼, 20 cm ■, 50 cm ★, 80 cm ●, 120 cm ◆; x = 5 cm ▬, 20 cm ▬, 50 cm ▬▬, 80 cm ▬·▬·▬, 120 cm - - -.

In this model, the bubble diameter is set equal to 1.8 mm which represents the average bubble diameter observed in the experiments.

Previous simulations of a bubbly wake with various interfacial momentum transfer models allowed to analyze the interfacial forces controlling bubbles migration. We kept in these simulations the same interfacial closure laws as in Chahed et al.[15] The lift is calculated with a coefficient (C_{LF} = 0.25), the added mass coefficient is C_A = 0.5, the turbulent stress tensor of the gas is set proportional to the liquid one through a proportionality factor fixed from the experimental data (see next paragraph), and the drag force is calculated with the following drag coefficient[34]:

$$C_D = \frac{2}{3}\text{Eö}^{0.5} \tag{14}$$

where Eö is the Eötvös number $\text{Eö} = g(\rho_l - \rho_g)d^2/\sigma$; σ is the surface tension (0.072 N m^{-1} for gas/water).

Mean flow: hydrodynamic and phase distribution

The injection of bubbles on just one side of the shear layer induces an acceleration of the bubbly side, and, due to the confinement and the conservation of mass, induces a deceleration of the single-phase side (Figure 4). A systematic acceleration of the bubbly side has been observed in various shear layer configurations. It is a buoyancy effect, where the bubbly side behaves like an equivalent lighter fluid.[8] This strong effect leads to a downstream evolution of the velocity difference across the mixing layer $\Delta U_L(x) = U_{L1}(x) - U_{L2}(x)$ (where $U_{L1}(x)$ and $U_{L2}(x)$ are the averaged velocities in the external cores defined as the regions where $\overline{\overline{u}}$ is nearly homogeneous in the transverse direction). In this flow, buoyancy leads to the inversion of the velocity gradient far from the inlet section. This behavior is globally well predicted by the two-fluid model. Detailed comparison between the experimental results and the numerical predictions is not perfect, but the longitudinal location of the inversion of the velocity profile, and the accelerations outside of the mixing zone are well reproduced. The small peak of the mean velocity located near y = 0 at the measuring sections near the inlet is due to a small nonuniformity of the injection system. It attenuates downstream and has no major effect because of the strong acceleration of the flow. In the last two sections of measurement, the transverse velocity of the fluid is over-estimated. To understand the buoyancy effect, we can rewrite the two-fluid momentum equations given for the gas–liquid flow (Eqs. 2 and 5), neglecting the viscous stress as compared to the turbulent correlations. The momentum equations (2) of the liquid then may be rewritten in the form:

$$\rho_L(1-\alpha)\frac{D\overline{\overline{u_{Li}}}}{Dt} = -\frac{\partial}{\partial x_i}\overline{\overline{p}} - \rho_L\frac{\partial}{\partial x_j}\left[(1-\alpha)\overline{\overline{u'_{Li}u'_{Lj}}}\right] + \rho_L(1-\alpha)g_i \tag{15}$$

Equation 15 shows up the fact that the liquid movement is submitted to a buoyancy force $\rho_L(1-\alpha)g_x$ which explains the acceleration of the bubbly side of the mixing layer along the x axis. Therefore, the accurate prediction of the transverse void fraction distribution is an important issue in the prediction of this bubbly flow.

We may indeed verify that the distribution of void fraction is quite well reproduced by the model (Figure 5). The simulation reproduces the transverse migration of the bubbles and the attenuation of the initial peak located at y = 0.02 m, which is the memory of the accumulation of the bubbles in the near wake of the splitter plate or of clustering in the shear layer near the inlet. Because of the decrease of $\Delta U_L(x)$ in the downstream direction, the capture of bubbles by large scales of the shear layer is not efficient enough to form clusters. Near the wall the model generates a peak of void fraction of about 6% which is expected,[35] but was not measured because we did not investigate the region near the wall.

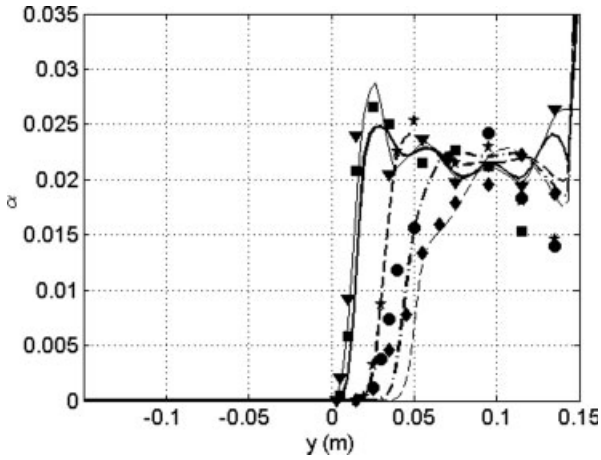

Figure 5. Void fraction profiles in the bubbly mixing layer.

X = 5 cm ▼, 20 cm ■, 50 cm ★, 80 cm ●, 120 cm ◆. Symbols, experimental results; lines, numerical prediction.

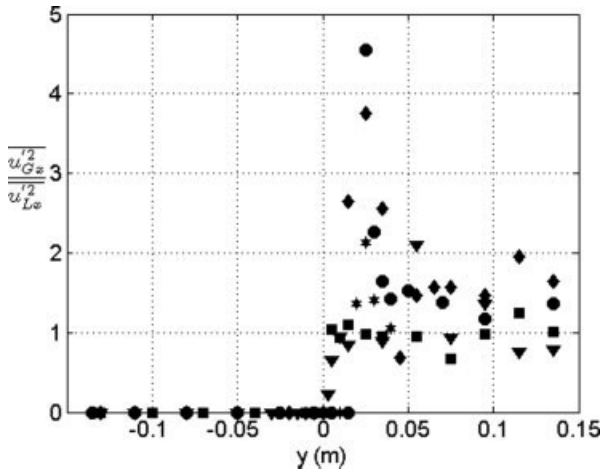

Figure 6. Ratio of the longitudinal variances of the velocities of both phases $\left(R_x = \overline{u'^2_{Gx}}/\overline{u'^2_{Lx}}\right)$.

Measurements $x = 5$ cm ▼, 20 cm ■, 50 cm ★, 80 cm ●, 120 cm ◆.

The quality of the prediction of the void fraction is strongly related to the model of the interfacial momentum transfer. In fact, the phase distribution in a bubbly flow is governed by the momentum transfer between the two phases as discussed in the following. With the closure of the momentum transfer given by Eq. 6, the momentum equation (5) of the gas writes:

$$0=\alpha\frac{\partial p}{\partial x_i}+\frac{3}{4}\alpha\rho_L\frac{C_D}{d}\|\overline{\overline{u_R}}\|\overline{\overline{u_{Ri}}}+2\alpha\rho_L C_{LF}\overline{\overline{\omega_{Lij}}}\times\overline{\overline{u_{Rj}}} +\alpha\rho_L C_A\left(\frac{d}{dt}\overline{\overline{u_{Gi}}}-\frac{D}{Dt}\overline{\overline{u_{Li}}}\right)\Big)+\rho_L C_A\frac{\partial}{\partial x_j}\left[\alpha\left(\overline{\overline{u'_{Gi}u'_{Gj}}}-\overline{\overline{u'_{Li}u'_{Lj}}}\right)\right] \tag{16}$$

According to Eq. 16, the force exerted by the liquid on the bubbles comprises the turbulent correlations issued from the added mass force on the bubbles. The turbulent contribution of the added mass force contains the turbulent correlations of the liquid and of the gas. So we have to provide closures not only for the turbulence in the liquid but also for the turbulence of the gas. In the present contribution we have a crude model for the turbulence of the gas phase. In a homogeneous bubble-induced turbulence even at low void fraction (2%), Tchen's theory of turbulent dispersion does not hold.[7] This is because the relation between the fluctuating motions of both phases is not only a problem of "one-way coupling" response of the bubbles to the liquid fluctuating excitation. The Lagrangian properties of the bubble-induced turbulence are moreover not known, and are undoubtedly strongly modified. In our experimental conditions, the bubble-induced turbulence is also noticeable, and we have thus just assumed that the kinetic tensor of the dispersed phase is proportional to the Reynolds tensor, which is reasonable. But we take a constant value for the proportionality ratio, which is a crude approximation. We used the experimental results obtained in the mixing layer to fix the order of magnitude of this ratio (Figure 6). We take for each diagonal component ($i \neq j$) $\overline{\overline{u'_{Gi}u'_{Gj}}}\Big/\overline{\overline{u'_{Li}u'_{Lj}}} = r$ with r equal to 3, and the shear stresses of both phases are taken equal.

The relative velocity of the bubbles is plotted on Figure 7. Its prediction results from the resolution of the momentum balances in both phases. But the numerical prediction stays very close to the terminal velocity, whatever the position of the bubbles, that is, whatever the spatial accelerations and gradients. Thus, the predicted relative movement is mainly associated to an equilibrium between the drag (whose coefficient is given in Eq. 14) and the buoyancy force on a bubble. Only the global value of the relative velocity compares favorably with the experimental results. The global evolution observed in the experimental measurements with the longitudinal position x, is related to the evolution of the diameters, and thus cannot be reproduced in our formulation. Moreover, the decrease of the experimental relative velocity in the region near $y = 0$ at section $x = 0.2$ m may be attributed to a plausible capture of the bubbles in the coherent structures of the mixing layer. It is not possible with our approach to model such detailed interactions. Because of the decrease of the velocity difference across the mixing layer, when x increases, the ability of the flow to generate and propagate coherent structures is undoubtedly destroyed, and such a capture is no longer present when x increases.

We also present a short discussion of the effects of the various terms involved in the interfacial transfer of momentum. Figure 8 presents the void fraction distribution predicted for various closure laws departing from the usual one defined previously and denoted case (c) in Figure 8. The void fraction is not so sensitive to the closure laws at the lowest sections of measurement. But far from the entrance ($x = 120$ cm), it is clear that taking into account only the drag force (case (a)) is not sufficient to predict the void fraction. The introduction of the averaged added mass force and its turbulent contribution (case (b)) alone is neither satisfactory, because the lift force, taken into account in case (c), participates to the transverse migration of the bubbles. In case (c) the coefficient for turbulent added mass force $r = 3$ is taken as a mean value from the experiments. We know that such a

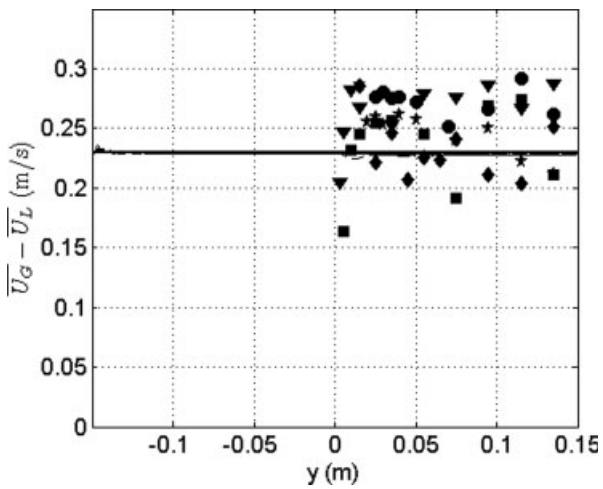

Figure 7. Average relative velocity of the bubbles in the mixing layer.

$X = 5$ cm ▼, 20 cm ■, 50 cm ★, 80 cm ●, 120 cm ◆. Symbols, experimental results; lines, numerical prediction.

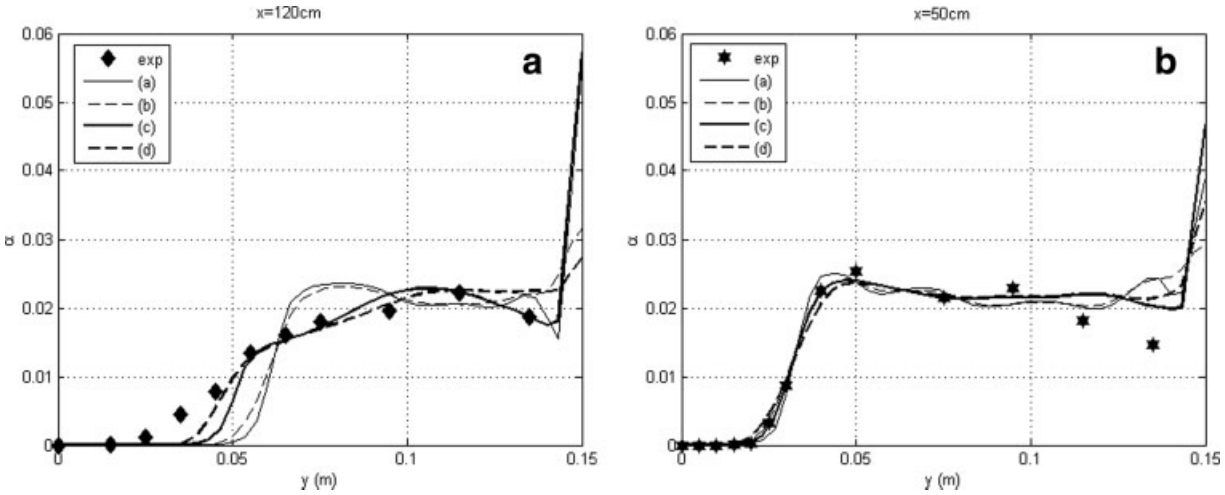

Figure 8. Sensitivity of the void fraction prediction to the closure laws for the interfacial transfer of momentum at positions $x = 50$ cm and 120 cm.

Symbols, experimental results; lines, numerical prediction with the following models: (a) $C_D = \frac{2}{3}\text{Eö}^{0.5}, C_A = 0, C_{LF} = 0, r = 1$, (b) $C_D = \frac{2}{3}\text{Eö}^{0.5}, C_A = 0.5, C_{LF} = 0, r = 2$, (c) $C_D = \frac{2}{3}\text{Eö}^{0.5}, C_A = 0.5, C_{LF} = 0.25, r = 3$, (d) $C_D = \frac{2}{3}\text{Eö}^{0.5}, C_A = 0.5, C_{LF} = 0.25$, r increases linearly with x between 3 and 9.

model for the turbulence in the gas phase is very crude. The experiments indicate that r increases with x (Figure 6), and the maximum value of r given by Tchen's theory is 9. So, we have also tested the effect of a linear evolution of this ratio r with the longitudinal direction, to take into account the evolution of the response of the bubbles to the turbulence in a flow where the turbulent length scales vary. This numerical simulation, denoted case (d) also improves the agreement with the void fraction measurements, and reveals that it is important to improve the modeling of the turbulent added mass force.

Turbulence in the liquid phase

The bubbly flows that we have investigated present deep modulations of the turbulence. Figure 9 shows that the measured turbulent kinetic energy is largely modified in the bubbly core of the flow as compared to the single-phase core because of the important contribution of the bubble-induced turbulence. Such a modification, as well as changes of the integral scales in turbulent bubbly flows, has already been observed in homogeneous bubbly flows or mixing layers.[7,29] The turbulence in the liquid results either from the production by the mean shear rate in the shear layer, and the memory of the inlet; or from the production by the bubbles, consisting mainly in the production by their relative movement. The effect of the production by the mean shear stress does clearly explain the presence of a peak of turbulence in the two first transverse profiles ($x = 5$ and 20 cm). But downstream the competition between the various mechanisms controlling the turbulence evolves due to the evolution of $\Delta U_L(x)$, and this introduces a key difficulty for the prediction of the turbulence which is typical of this particular bubbly flow configuration. The maximum of turbulent kinetic energy disappears when $\Delta U_L(x)$ vanishes. In the downstream sections the turbulence is dominated by bubble-induced turbulence.

The numerical results reproduce quite well the amount of the turbulent kinetic energy in the bubbly mixing layer. The turbulent energy k produced by the model is compared to the longitudinal turbulent kinetic energy $\frac{3}{2}\overline{\overline{u_{Lx}'^2}}$ due to a lack of measurements of the transverse components of the velocity of the fluid. Figure 9 shows that the turbulence model is able to predict with a quite good agreement as well the turbulent kinetic energy in the two-phase external core of the mixing layer as well as in the single-phase one. The discrepancy between the numerical results and the experimental data in the sheared region at $x = 20$ cm may be related to the overestimation of $\Delta U_L(x)$ in the numerical prediction. But a gen-

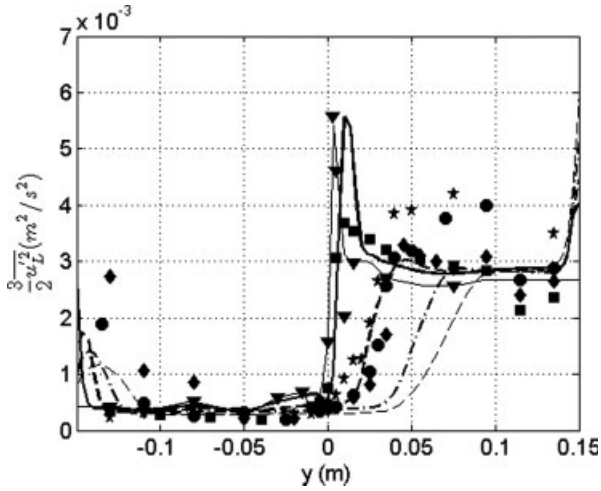

Figure 9. Turbulent energy profiles in the bubbly mixing layer.

$X = 5$ cm ▼, 20 cm ■, 50 cm ★, 80 cm ●, 120 cm ◆. Symbols, experimental results $\frac{3}{2}\overline{\overline{u_{Lx}'^2}}$; lines, numerical prediction of the fluctuating kinetic energy k.

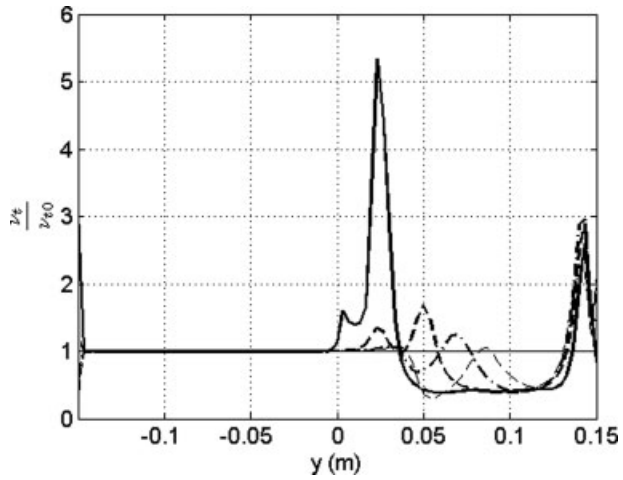

Figure 10. Turbulent viscosity profiles in the bubbly mixing layer.

Numerical prediction at $x = 5$ cm ▬, 20 cm ▬, 50 cm ▬ ▬, 80 cm ▬ · ▬ · ▬, 120 cm ▬ ▬.

eral trend is correctly predicted: downstream the numerical model predicts the attenuation and the transverse displacement of the peak of k in agreement with the experimental results. To obtain such a result, the whole turbulence model is necessary. The improvements of the turbulence modeling, particularly concerning the decomposition of the turbulent energy in turbulent and pseudo-turbulent contributions, make possible the computation of the scales involved in each region of the flow, and allow the model to describe the effects of the bubbles agitation on the turbulent shear stress. Figure 10 shows the predicted turbulent viscosity divided by ν_{t0}. The important values and variations of this ratio indicates the important role of the scales involved in the relation (Eq. 7) giving the turbulent viscosity and thus its effect on the turbulent shear stress. Unfortunately, we have no experimental data on the turbulent shear stress to discuss these numerical results. But the correct concordance between the numerical results and experimental data concerning the average velocity fields indicates that the turbulent shear stress is reasonably predicted. The under-estimation of the turbulence in the external core regions from $x = 80$ cm by numerical simulation can be attributed for a part to the fact that we compare the predicted value of k and the experimental value $\frac{3}{2}\overline{u'^2_{Lx}}$ or may be to a lack in the closure of the interfacial source term of Eq. 10 for the pseudo-turbulent kinetic energy which proved to be negligible.

Turbulent scalar transport and mass transfer

The profiles of the concentration of dissolved oxygen in the liquid are reported on Figure 11. The interfacial mass transfer leads to the increase of the level of this concentration in the external bubbly core of the flow. A global transverse displacement towards the bubbly side is also observed. It is related to the transverse migration of the bubbles, and to the transverse convection of the passive scalar in the liquid phase. In the last two sections of measurements the predicted concentration profiles are displaced laterally as compared to the experimental results. This is an effect of an over-prediction of the transverse convective transport by the liquid. For $y > 0.12$ m, and $x > 0.2$ m, the prediction of the concentration is not satisfactory due to the effect of the wall. However, the model reproduces globally the concentration field of the dissolved oxygen. The mechanisms for scalar transport and mass transfer are taken into account but improvements of the closure laws are necessary.

In this model, the interfacial mass transfer closure law is controlled by the length and time scales of the relative movements of the bubbles (Eq. 13). We have also tested the model of Higbie used in chemical engineering: $\mathrm{Sh} = \frac{2}{\sqrt{\pi}}\mathrm{Re}^{0.5}\mathrm{Sc}^{0.5}$. It proved to over-estimate the mass transfer (Figure 12). In the general case, due to the presence of numerous velocity and length scales in bubbly flows, one can expect that a more general model is needed for interfacial mass transfer. But for our flow conditions, with a low void fraction, and an important bubble-induced turbulence, the interfacial transfer rate given by Eq. 13 are satisfactory. In Figure 12 we have also reported some simulations using relation (Eq. 13) given by Brauer[26] for the mass transfer rate, but varying the bubble diameter. The results are not very sensitive to the value of the bubble diameter in the range 1.6–1.9 mm, and are in satisfactory agreement with the experimental results.

Conclusion

In this contribution, we have reported new experimental results characterizing the local hydrodynamics and mass transfer in a complex flow consisting in a buoyant bubbly shear layer. This flow contains strong variations of the void fraction, important accelerations, and regions of deeply contrasted turbulence (in the single-phase part, in the shear layer and in the bubbly core). The two-fluid Euler–Euler model that we have used is nevertheless able to reproduce the complex hydrodynamics of this bubbly flow, and gives satisfactory prediction of the dissolved oxygen concentration.

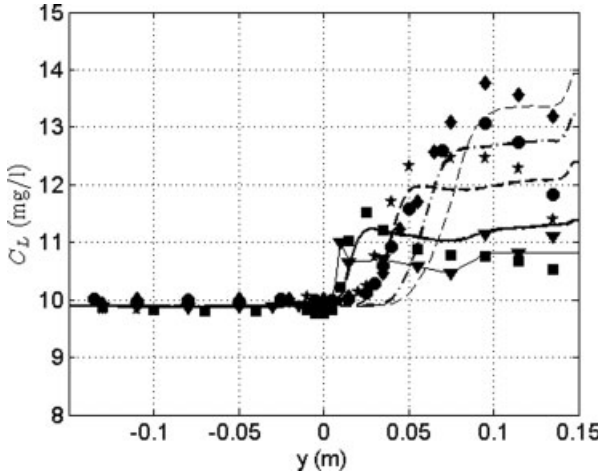

Figure 11. Profiles of the dissolved oxygen concentration in the bubbly mixing layer.

$X = 5$ cm ▼, 20 cm ■, 50 cm ★, 80 cm ●, 120 cm ◆. Symbols, experimental results; lines, numerical prediction.

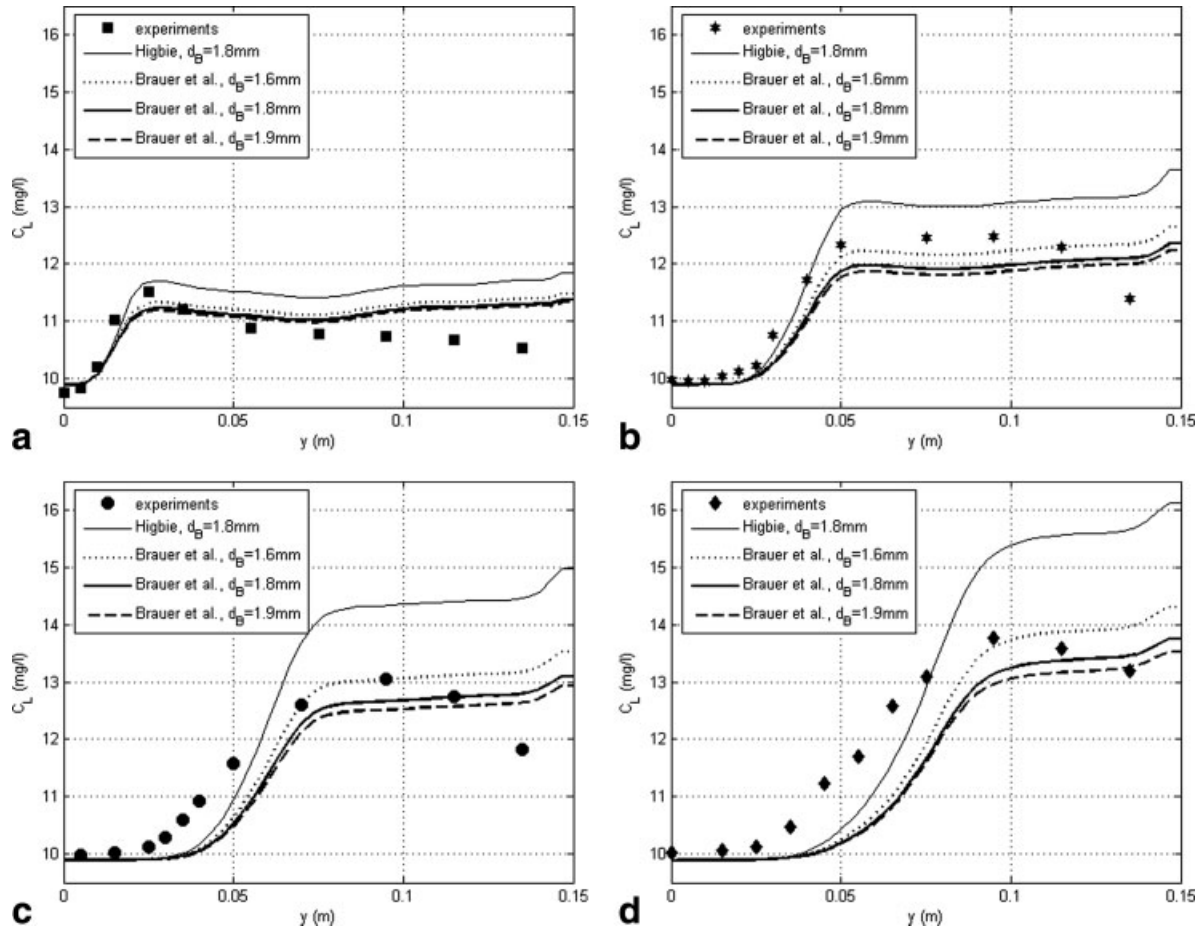

Figure 12. Profiles of the dissolved oxygen concentration in the bubbly mixing layer.

x = 20 cm (a), 50 cm (b), 80 cm (c), 120 cm (d). Symbols, experimental results; lines, numerical prediction with the models of Higbie or of Brauer[26] and various bubble diameters.

Some important questions still open to discussion will be developed in future work. One concerns the research of a more general scaling of the interfacial mass transfer. The mass transfer coefficient involves local time scales in relation with the mechanisms that control the interfacial transfer. For instance Higbie model involves time scale related to the bubble displacement. Nevertheless, the effect of turbulence, of bubble deformation, and of impurities are not yet completely explored even though some formulations based on turbulent time scales were proposed for stirred gas–liquid systems and validated against experimental investigations. In flows where turbulence originating from the mean shear stress and bubble-induced turbulence are in competition and interaction, it will be important to propose models taking into account simultaneously the scales associated to both mechanisms. Some experiments in bubbly shear layers with stronger shear-induced turbulence are planned to discuss this point.

Notation

a = interfacial area
C_A = added mass coefficient
C_D = drag coefficient
C_{LF} = lift coefficient
C_L = oxygen concentration in the liquid
C_L^* = concentration of oxygen in the liquid at saturation
d = mean bubble diameter
D = gas-liquid molecular diffusivity
Eö = Eötvös number
g_i = I component of the gravity
H = constant of Henry
k_0 = turbulent kinetic energy
k_L = mass transfer coefficient
k_S = kinetic energy of the pseudo-turbulence
M_{Gi} = i component of the interfacial momentum transfer rate form the gas to the liquid
p_L = pressure in the liquid phase
Re = Reynolds number of the relative movement
S_c = interfacial mass transfer
Sc = Schmidt number
Sh = Sherwood number
u_{ki} = i component of the velocity of phase k
$\overline{u_{ki}}$ = i component of the averaged velocity of phase k
U_{L1}, U_{L2} = averaged velocities in the external cores of the shear layer
$\overline{u_{R_i}}$ = mean relative velocity
U_R = norm of the relative velocity
$\overline{\overline{u'_{Li}u'_{Lj}}}$ = component of the Reynolds tensor of the liquid (k = L) or of the kinetic tensor (k = G)
$\overline{\overline{u'_{Li}u'_{Lj}}}\,(0)$ = turbulent part of the Reynolds tensor produced by the gradient of the mean velocity and by the bubbles' wakes
$\overline{\overline{u'_{Li}u'_{Lj}}}\,(S)$ = pseudo-turbulent part of the Reynolds tensor induced by the bubbles displacements
α = void fraction, gas hold-up

α_k = volumetric fraction of phase k
ε_0 = viscous dissipation rate
χ_k = characteristic function of phase k
μ_k = dynamic molecular viscosity of phase k
ν = molecular viscosity of the liquid
ν_t = turbulent viscosity
ν_{t0} = asymptotic turbulent viscosity (when $k_s \rightarrow 0$ and $\tau_b >> \tau_t$)
ρ_k = density of phase k
σ = surface tension
σ_{kij} = stress tensor of phase k
$\sigma_{Lij}^{(0)}$ = stress tensor of the "non-perturbed" liquid flow
τ_b = characteristic times scale of the relative movement
τ_t = characteristic times scale of the turbulence
$\overline{\overline{\omega_{Lij}}}$ = mean vorticity of the liquid

Literature Cited

1. Lain S, Bröder D, Sommerfeld M. Experimental and numerical studies of the hydrodynamics in a bubble column. *Chem Eng Sci*. 1999;54:4913–4920.
2. Cockx A, Do-Quang Z, Liné A, Roustan M. Use of computational fluid dynamics for simulating hydrodynamics and mass transfer in industrial ozonation towers. *Chem Eng Sci*. 1999;54:5085–5090.
3. Buscaglia GC, Bombardelli FA, Garcia MH. Numerical modeling of large-scale bubble plumes accounting for mass transfer affects. *Int J Multiphase Flow*. 2002;28:1763–1785.
4. Sokolichin A, Eigenberger G, Lapin A. Simulation of buoyancy driven bubbly flow: established simplifications and open questions. *AIChE J*. 2004;50:24–45.
5. Sundaresan S. Modeling the hydrodynamics of multiphase flow reactors: current status and challenges. *AIChE J*. 2000;46:1102–1105.
6. Koynov A, Khinast JG, Tryggvason G. Mass transfer and chemical reactions in bubble swarms with dynamic interfaces. *AIChE J*. 2005;51:2786–2800.
7. Larue de Tournemine A. Etude expérimentale de l'effet du taux de vide en écoulements diphasiques à bulles, PhD Dissertation. France: Institut National Polytechnique de Toulouse, 2001.
8. Larue de Tournemine A, Roig V.Etude d'une couche de mélange diphasique à bulles confinée en présence d'effets de flottabilité. In: *Proceedings of the Congrès Français de Mécanique*, Nice, 2003.
9. Chahed J, Roig V, Mabernat L. Eulerian–Eulerian two-fluid model for turbulent bubbly flows. *Int J Multiphase Flow*. 2003;29:23–49.
10. Bellakhal G, Chahed J, Masbernat L. k-Omega turbulence model for bubbly flows. In: *Proceedings of the 5th International Conference on Multiphase Flow, ICMF'05*, Yokohama, Japan, May 30–June 4, 2004. Paper No. 319.
11. Bellakhal G, Chahed J, Masbernat L. Analysis of the turbulence structure in homogeneous shear bubbly flow using a turbulent viscosity model. *J Turbulence*. 2004;36:16.
12. Sato Y, Sadatomi L, Sekoguchi K. Momentum and heat transfer in two-phase bubbly flow. *Int J Multiphase Flow*. 1981;7:167–190.
13. Lopez de Bertodano M, Lee SJ, Lahey RT, Jones OC. Development of a k-ε model for bubbly two-phase flow. *J Fluids Eng*. 1994;116:128–134.
14. Serizawa A, Kataoka I, Michiyoshi I. Phase distribution in bubbly flow. In: Hewitt GF, Delhaye JM, Zuber N, editors. *Multiphase Science and Technology, Vol. 6*. Washington, DC: Hemisphere Publishing Corporation 1992:257–301.
15. Chahed J, Colin C, Masbernat L. Turbulence and phase distribution in bubbly pipe flow under micro-gravity condition. *J Fluids Eng*. 2002;124:951–956.
16. Drew DA, Lahey RT. Phase distribution mechanisms in turbulent low-quality two phase flow in circular pipe. *J Fluid Mech*. 1982;117:91–106.
17. Bel F'Dhila R, Simonin O. Eulerian prediction of a turbulent bubbly flow downstream of a sudden pipe expansion. In: *Proceedings of the 6th Workshop on Two-Phase Flow Predictions*, Erlangen, Germany, March 30–April 2, 1992.
18. Lance M, Lopez de Bertodano M. Phase distribution phenomena and wall effects in bubbly two-phase flows. In: *Proceedings of the Third International Workshop on Two-Phase Flow Fundamentals*, Imperial College, London, June 15–19, 1992.
19. Oey RS, Mudde RF, van den Akker HEA. Sensitivity study on interfacial closure laws in two-fluid bubbly flow simulations. *AIChE J*. 2003;49:1621–1636.
20. Chahed J, Masbernat L, Bellakhel G. k-ε Model for bubbly flow. In: *Proceedings of the 2nd Symposium on Two-Phase Flow Modelling and Experimentation*, Pisa-Italy, 1999.
21. Maxey R, Riley J. Equation of motion for a small rigid sphere in non-uniform flow. *Phys Fluids*. 1983;26:883–889.
22. Gatignol R. The Faxen formulae for a rigid particle in an unsteady non-uniform stokes flow. *J Mécanique Théorique Appliquée*. 1983;9:143–160.
23. Liu TJ, Bankoff SG. Structure of air–water bubbly flow in a vertical pipe. I. Liquid mean velocity and turbulence measurements. *Int J Heat Mass Transfer*. 1990;36:1049–1060.
24. Biesheuvel A, Van Wijngaarden L. Two-phase flow equation for a dilute dispersion of gas bubbles in liquid. *J Fluid Mech*. 1984;148:301–318.
25. Lance M, Bataille J. Turbulence in the liquid phase of a uniform bubbly air water flow. *J Fluid Mech*. 1991;222:95–118.
26. Brauer H. Particle/fluid transport processes. *Prog Chem Eng*. 1979;17:61–99.
27. Mewes D, Wiemann D. Two-phase flow with mass transfer in bubble columns. *Chem Eng Technol*. 2003;26:862–868.
28. Roig V, Larue de Tournemine A. Measurement of interstitial velocity of homogeneous bubbly flows at low to moderate void fractions. *J Fluid Mech*. 2007;572:87–110.
29. Roig V, Suzanne C, Masbernat L. Experimental investigation of a turbulent bubbly mixing layer. *Int J Multiphase Flows*. 1998;24:35–54.
30. Clark NN, Turton R. Chord length distributions related to bubble size distributions in multiphase flow. *Int J Multiphase Flow*. 1988;14:413–424.
31. Simonin O. Eulerian formulation for particle dispersion in turbulent two-phase flows. In: Sommerfeld M, Wennerberg D, editors. *Proceedings of the Fifth Workshop on Two-phase Flow Predictions*. Erlangen, Germany, 1990:156–166.
32. Simonin O, Viollet PL. Modelling of turbulent two-phase jets loaded with discrete particles. In: Hewitt FG, et al., editors. *Phase-Interface Phenomena in Multiphase Flows*. Washington, DC: Hemisphere Publishing Corporation 1990:259–269.
33. Simonin O, Viollet PL. Prediction of an oxygen droplet pulverization in a compressible subsonic co-flowing hydrogen flow. Symposium on Numerical Methods for Multiphase Flows, Jan. 4–7, 1990, Toronto, Canada.
34. Ishii M, Mishima K. Two-fluid model and hydrodynamic constitutive relations. *Nucl Eng Des*. 1984;82:107–126.
35. Marié JL, Moursali E, Tran-Cong S. Similarity law and turbulence intensity profiles in a bubbly boundary layer at low void fractions. *Int J Multiphase Flow*. 1997;23:227–247.

Manuscript received Nov. 6, 2006, and revision received July 16, 2007.